Novel synthesis of thick wall coatings of titania supported Bi poisoned Pd catalysts and application in selective hydrogenation of acetylene alcohols in capillary microreactors

Nikolay Cherkasov[a], Alex O. Ibhadon[a*], Evgeny V. Rebrov[b]

[a] Catalysis and Reactor Engineering Research Group, Department of Chemistry and School of Biological, Biomedical and Environmental Sciences, University of Hull, Cottingham Road, Hull, HU6 7RX, United Kingdom

[b] School of Engineering, University of Warwick, Coventry, CV4 7AL, United Kingdom

[*] Corresponding author: a.o.ibhadon@hull.ac.uk

TOC image

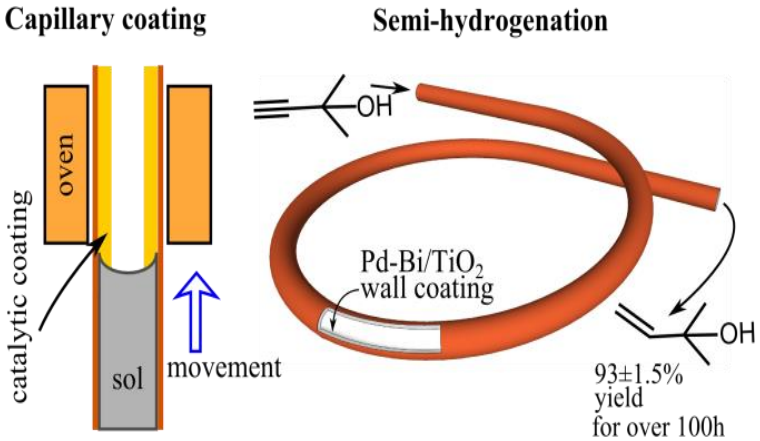

A novel synthesis method for thick coatings inside long capillary reactors was reported and applied to the semihydrogenation of 2-methyl-3-butyn-2-ol

Abstract

Catalysis in microreactors allows reactions to be performed in a very small volume, reducing the environmental problems and greatly intensifying the processes through easy pressure control and the elimination of heat- and mass- transfer limitations. In this study, we report a novel method for the controlled synthesis of micrometre-thick mesoporous TiO_2 catalytic coatings on the walls of long channels (>1 m) of capillary microreactors in a single deposition step. The method uses elevated temperature and introduces a convenient control parameter of the deposition rate (displacement speed controlled by a stepper motor), which allows deposition from concentrated and viscous sols without channel clogging. A capillary microreactor wall-coated with titania supported Bi-poisoned Pd catalyst was obtained using the method and used for the semihydrogenation of 2-methyl-3-butyn-2-ol providing 93±1.5 % alkene yield for 100 h without deactivation. Although the coating method was applied only for TiO_2 deposition, it is nonetheless suitable for the deposition of volatile sols.

Introduction

Mesoporous metal oxide coatings have many applications in photocatalysis, gas chromatography, electronics and many other areas.[1–7] In particular, they play an important role as catalysts or catalyst supports for microfluidic applications where a reaction is performed in a microreactor with the volume smaller than a millilitre. Microreactors have many advantages over traditional large-scale chemical reactors: the small dimensions of microreactors facilitate mass- and heat- transfer, small reaction volume allows the handling of hazardous or expensive chemicals safely and high-pressure reactions to be carried out with inexpensive equipment, hence significant process intensification is possible with microreactor technology.[8–14]

In heterogeneous catalytic reactions however, the advantages of microreactors are offset by the problem of catalyst introduction into the reactor. A convenient laboratory practice to use packed-bed reactors, *i.e.* fill the microreactor with the particles of supported catalysts, is possible in microreactors. However, great care should be taken to ensure that the catalyst particles do not block the channels and that mass and heat transfer limitations do not apply.[15–18] A slurry of catalyst nanoparticles can be introduced into a flow reactor to overcome the problems of clogging and mass-transfer, but this approach creates a problem of catalyst separation from the product at the end of the reaction.[19] Hence, the most convenient way of performing catalytic reactions in flow systems is to coat the reactor walls

with a catalyst. The coating can be done by grafting the reactor walls with metallorganic molecules, but this approach requires very expensive chemicals and complex synthesis procedures.[20] A more common approach is the deposition of metallic catalysts supported on oxide materials. There are well-developed methods of introduction of catalytically active metal nanoparticles into oxide matrixes, but subsequent deposition of the matrix uniformly on the reactor walls is still a very challenging task, especially for concentrated sols and long reactors.[21–23]

Two main methods are used to obtain a uniform coating on a substrate: spin- and dip- coating. In the spin-coating technique, the substrate is first covered with an excess of precursor solution that is later removed by centrifugal forces leaving a thin uniform coating after solvent evaporation.[24] Thus, spin-coating is suitable only for flat or slightly curved surfaces and cannot be used to create coatings inside capillary channels. The dip-coating method on the other hand, is also traditionally applied to flat substrates that are submerged and withdrawn from a solution containing a precursor of metal oxide in a volatile solvent.[24] Depending on the withdrawing speed, three deposition regimes can be observed: the capillary, the draining or a combination of both regimes.[25] The capillary regime is observed for very slow withdrawing speeds (<0.1 mm/s) and is associated with the capillary rise in the formed solid film. The draining regime, on the contrary, dominates at high withdrawing speeds (> 1mm/s) due to quick dragging of the viscous fluid. For a given system, the conditions that separate these regimes and the resulting coating thickness is determined by a combination of liquid viscosity, surface tension and most importantly, the liquid evaporation rate.[25] By careful optimisation of the dip-coating conditions, very fine control of the coating can be achieved as demonstrated by Krins *et al.*,[26] who obtained a crack-free TiO_2 coating with a thickness of up to 0.5 μm in a single deposition stage.

A method similar to dip coating adapted for tubular substrates, is called the gas displacement method. A horizontal tube to be coated is first filled with the precursor solution, then gas displaces the liquid leaving some liquid along the walls.[27] This method was applied to obtain a 5-20 μm thick coating inside shorter (0.3 m) reactors[28] or a thin coating (90 nm) inside 10-m long reactors.[23,29] Another derivative of the dip-coating method, the fill-and-dry method, can be used to obtain 10-20 μm thick catalytic coatings inside short reactors.[30–32]

However, the essential component of these methods, solvent evaporation, requires years to remove solvent from a longer (5 m) reactor according to estimations performed using Stefan's equation,[33] Fig. 1. As expected, evaporation time decreases at high vapour pressure, *i.e.* close to the boiling point of the solvent, however, the shortest evaporation time observed in the presented parameter range, 1.3 years, is still unacceptably high and requires very tight temperature control. Clearly, a 1000-fold

increase in the evaporation rate, which is needed to perform the coating within several hours, cannot be achieved by simply changing the solvent. Therefore, the solvent removal from the reactor should be performed under unsteady conditions.

Fig. 1. Effect of temperature and pressure on the evaporation time of the 5-m long reactor filled with ethanol, estimated using Stefan's equation.[33]

Static and dynamic coating methods were developed for chromatographic applications and addressed the problem of solvent evaporation. With dynamic coating, a plug of the precursor solution is pushed through the reactor leaving some solution on the column walls. The solution is later dried by passing excess gas through the capillary. Static coating implies filling the reactor with a precursor solution, closing one end of the capillary and applying vacuum to the other end to facilitate evaporation.[34,35] The static coating method offers a simple way of achieving uniform coating synthesis with a thickness that can be adjusted by changing the precursor solution concentration.[35–37] Other experimental parameters such as the evaporation temperature and the pressure should be optimised to slow the evaporation rate required to obtain uniform coatings. However, if thick coatings are to be obtained, the concentration of the precursor solution should be increased. This leads to increased viscosity, greatly limits the range of adjustable parameters, decreases evaporation rate, and significantly raises the probability of plug formation inside the capillaries.[36,37] Hence, the preparation of long microreactors with thick catalytic coatings is still a very challenging task.

In this work, a novel sol-gel-based method is reported for the synthesis of metal oxide coatings suitable for long capillary microreactors. The method is similar to the static coating method, but uses elevated temperature and introduces an additional external parameter, displacement speed, that controls the deposition rate. In order to demonstrate the application of the method in the synthesis of catalytic coatings, the liquid phase semihydrogenation of 2-methyl-3-buyne-2-ol (MBY) to 2-methyl-3-buten-2-ol (MBE) was selected because of the precise reaction control that is needed to stop the reaction at the alkene stage and the importance of this reaction in the synthesis of many fine chemicals such as vitamins (A, E), and fragrances (Linalool).[38] Traditionally, semihydrogenation reactions are performed in batch reactors with lead-containing Lindlar catalysts, where lead blocks some active sites and affects the adsorption energy of intermediate species, improving the alkene yield.[39,40] However, the high toxicity of lead raises environmental concerns and as a result, Bi was used as a doping agent, a notably

less toxic metal.[41] In addition, the synthesis of Bi-poisoned Pd catalyst is simple, meaning low catalyst costs.[40,42]

Experimental section

TiO_2 sol preparation

A titanium dioxide sol was prepared using an established method by hydrolysis of titanium alkoxide solution.[43] Hot distilled water (360 K, 8.1 g) was quickly added to a solution of 20.2 g titanium (IV) butoxide (Sigma-Aldrich, 97 wt. %) in 6.60 g of methanol (Fisher Scientific, 99.9 wt. %) under vigorous stirring to obtain TiO_2 particles (hydrolysis ratio $[H_2O]/[Ti]=15$). After 15 min of stirring, 0.78 g of concentrated HNO_3 (Fisher Scientific, 65 wt. %) was added to disperse any agglomerated TiO_2 and the dispersion was refluxed for 4 h. Pluronic F127 surfactant (Sigma-Aldrich), 1.0 g, was added and the solution was left stirring for 2 h at room temperature. The dispersion obtained was left in an ultrasonic bath for 20 min and diluted with methanol to obtain titania sols with concentrations ranging from 5 to 80 g/L.

Synthesis of TiO_2 coatings

The coating apparatus consists of a stepper motor, controlled by an Arduino microcontroller, which pushes the capillary vertically at a constant velocity into the oven, Fig. 2. The capillary is guided into the oven by a 3 mm coiled copper tubing insulated with ceramic wool for the first 5 cm that allows gradual temperature increase along this length. The total length of the copper guide is longer than that of the capillary to ensure that the capillary is held at high temperature to prevent condensation of the solvent within the capillary.

Fused silica capillaries with internal diameter of 250 μm were used unless otherwise stated. Prior to the coating deposition, the capillaries were activated by passing the following solutions at 20 μL/min for 15 min: water, a 1 M NaOH solution, water, a 2 M $Na_2Cr_2O_7$ in 5 M H_2SO_4 solution and water. The capillary (0.5-1 m long) was then slowly (7 μL/min) filled with the titania sol using a syringe pump and the free end of the capillary was closed with a shut-off valve. The first 5 cm of the capillary was left without the dispersion to minimise clogging during the initial stages of the coating. The filled capillary was displaced into the oven at a constant linear velocity (displacement speed) of 0.1-10 mm/s by the stepper motor (step length 20 μm).

Fig. 2. Schematic view of the coating apparatus.

The capillaries obtained left at 473 K in a vacuum oven for 10 h to stabilise the coating, flushed with ethanol at 300 μL/min for 20 min to remove any loose fragments of the coating and to extract the surfactant. The capillaries were then dried at 390 K in air. At least, three identical capillaries were coated using the same method to ensure the reproducibility of the method.

To obtain enough material for characterisation, a glass tube with an internal diameter of 1.5 mm was also coated with the 80 g/L titania sol using the method described above. The coating obtained was mechanically removed and used for further characterisation.

Synthesis of the Pd-Bi/TiO_2 coatings

The selective poisoning of Pd active sites with Bi was performed by adapting the method of Anderson and co-workers.[40,42] Unsupported Bi-poisoned palladium nanoparticles were synthesised by reducing 45 mg of palladium (II) acetate (Sigma-Aldrich, 98 wt. %) in the presence of 250 mg of polyvinylpyrrolidone (Sigma-Aldrich) which were dissolved in 15 mL of methanol. A solution of 20 mg sodium borohydride (Sigma-Aldrich, 98 wt. %) in 5 mL of methanol was quickly added and left stirring for 1 h. Any excess of sodium borohydride was neutralised by adding 0.2 ml of acetic acid (Fisher Chemical, 99 wt. %). Afterwards, 1.7 mL of an aqueous 0.02 M $Bi(NO_3)_3$ solution in 2% acetic acid was added to the dispersion obtained with stirring for 3 h at 320 K in hydrogen atmosphere (1 bar). The solvent was evaporated using a rotary evaporator until the total solution volume reached 7 mL.

The Pd-Bi nanoparticle dispersion was mixed with the 80 g/L TiO_2 sol in 1:1 volume ratio and left in an ultrasonic bath for 20 min. The dispersion obtained was used to fill a 2.5 m fused silica capillary (0.53 mm internal diameter) and prepare a coating as described above using a displacement velocity of 0.2 mm/s and the oven temperature of 450 K.

Semihydrogenation

A schematic view of the hydrogenation apparatus is shown in Fig. 3. It consists of two mass-flow controllers (Aalborg) for hydrogen and nitrogen (CK gas, 99.999 vol. %), a continuous-flow syringe pump (SyrDos2) connected with a T-joint to the capillary microreactor. The capillary was placed in a temperature-controlled water bath and connected to a sample collector. The residence time in the reactor was estimated by injection of a pulse of octane 10 μL (Alfa Aesar, 99 vol. %) into the T-joint

and analysing its concentration at the reactor outlet. At the liquid flow rate of 40 μL/min, the average residence time was determined by pulsing methylene blue to be 120 s, which agrees with the Lockhart-Martinelli correlation.[44,45] The semihydrogenation of 2-methyl-3-butyn-2-ol (MBY, Sigma-Aldrich, wt. 98 %) was performed using a 1200 mol/m^3 MBY solution in hexane (VWR, 98 wt. %). The reaction conditions were optimised in the temperature range from 310 to 335 K, hydrogen flow rate of 10 mL/min (STP) and a solution flow rate of 30-50 μL/min. During the optimisation, the experimental conditions were set, the system was allowed to reach a steady state within 30-60 min, then 3-5 samples were collected (100 μL) within 3 h of operation. The samples were diluted in a 1:10 ratio with hexane and analysed using a Varian 430 gas chromatograph fitted with an autosampler and a 30 m Stabiwax capillary column.

Fig. 3. Scheme of the hydrogenation apparatus

Characterization of TiO_2 coatings

Scanning electron microscopy analysis

Scanning electron microscopy (SEM) study was performed using a TM-1000 Hitachi Tabletop Microscope. The capillary was cut into 4 mm sections evenly distributed along the capillary length. These sections were vertically glued on a sample holder. For every capillary, up to 30 individual cross-sections were studied measuring between 10 and 20 positions along the angular direction for analysis of thickness distribution.

Pressure drop analysis

The hydrodynamic diameter of the coated capillaries was calculated from the Hagen–Poiseuille equation. In these experiments, ethylene glycol was fed at a desired flow rate in the range of 50 to 300 μL/min and the pressure drop was measured with a pressure transducer (Alicat PC100). The viscosity of the ethylene glycol at room temperature was determined using an untreated capillary with a diameter of 250 μm±0.7μm. The thickness of the coating was calculated as the difference between the initial diameter and the hydraulic diameter of the coated capillary.

BET and PXRD measurements

The surface area and pore size distribution of the titania coatings were measured from N_2 adsorption-desorption isotherms (Energas, 99.999 vol. %) using a TriStar 3000 micrometrics analyser using standard multipoint BET analysis and BJH pore distribution methods. Prior to nitrogen adsorption, the material was dried in nitrogen flow at 410 K for 3 h. PXRD patterns were recorded using an Empyrean powder X-ray diffractometer equipped with a monochromatic Kα-Cu X-ray source in the 2θ range 20-80^o, step size 0.039^o and step time 180 s. The patterns obtained were analysed using PANalytical Highscore Plus software.

Results and Discussion

Titania coated capillary reactors

Metal oxide sols in high concentrations present many practical problems for the coating process. Firstly, these sols are very viscous non-Newtonian fluids that easily clog the capillaries on deposition.[28] Secondly, the boiling points of methanol and butanol of 338 and 390 K, respectively, require a temperature above 395 K for complete solvent removal. However, controlled and slow solvent evaporation at high temperature is very difficult due to vigorous solvent boiling. The method reported in this work addresses these problems by using an elevated temperature and pressure as opposed to conventionally used vacuum-based techniques.[34–37] The temperature of the copper guide tubing at the entrance to the oven (Fig. 2) increases linearly from about 350 K (air-cooled side) to the oven temperature. Hence, when the capillary is moving into the oven, its temperature gradually increases leading to the preferential evaporation of the most volatile components in the solution followed by full evaporation.

The method offers several adjustable experimental parameters such as the titania sol concentration, the temperature of the oven and the displacement speed. Aiming for the highest coating thickness, a titania sol with a concentration of 80 g/L was used in the parametric study. First, the capillaries were coated at oven temperatures of 390, 420 and 450 K and a displacement speed of 0.1 mm/s. At the temperatures of 390 and 420 K, the capillaries were clogged by a solid deposit, while at 450 K the deposition process was reproducible and the coating thickness was uniform along the length. The absence of clogging at 450 K might be due to (i) the decreased viscosity at the higher temperature, and importantly, (ii) higher vapour pressure. Because methanol vapour pressure is 14 and 27 bar at 420 and 450 K, respectively,

the removal of a plug formed inside the capillary is more likely at a higher temperature due to pressure build up.

Fig. 4a shows a typical SEM image of the cross-section and the pore size distribution (PSD) of a 250 μm capillary coated with a 4 μm-thick layer of titania obtained in a single deposition stage. A mean pore size of 5.7 nm was observed. The coating consisted of two phases of TiO_2: anatase and brookite in a 30/70 ratio according to the PXRD data (Fig. 4b). The crystallite size of the sol was relatively small (5.1±1.8 nm estimated using Williamson-Hall plot) due to high hydrolysis ratio used for sol preparation.[43]

Fig. 4. (a) PSD of the TiO_2 coatings, (insert) SEM image of the cross-section of the titania coated 250 μm capillary, and (b) the PXRD pattern of the coating.

In the deposition method, the displacement speed serves as a convenient external control parameter of the evaporation rate. At a displacement speed above 5 mm/s, the coating thickness was not constant in the angular direction (Fig. 5a). However, at a displacement speed below 0.2 mm/s, the coating thickness was uniform with random deviations from the mean value (Fig. 5b). At an intermediate displacement speed, the thickness distribution of the coatings along the capillary circumference was intermediate between these two cases. The non-uniform coating along the angular direction can be explained considering that at high displacement speed, there was not enough time for the solvent to evaporate in the vertical part of the guide tubing. Hence, solvent evaporation took place at the bend or in horizontal section (Fig. 2), which led to a spreading of the sol at the capillary bottom by gravitational forces. At low displacement speed, the evaporation rate was slow enough so the solvent evaporation took place in the vertical section forming a uniform coating.

Fig. 5. Cross-sectional SEM images of the capillaries coated at (a) 0.2 mm/s, (b) 5 mm/s and the coating thickness as a function of angular position.

The effect of sol concentration on the coating properties was studied at a displacement speed of 0.2 mm/s and a sol concentration ranging from 5 to 80 g/L. In these cases, the distribution of the coating thickness in the angular direction was uniform as in Fig. 5b, while the axial thickness changed with concentration. Fig. 6a shows the axial thickness distribution determined by studying cross-sectional

SEM images. As expected, the coating thickness increased at higher sol concentrations, because more titania was introduced into the capillaries. Fig. 6b shows a comparison of the average coating thickness determined using the SEM images and hydrodynamic measurements. These data on the coating thickness are in good agreement (considering standard deviation of the experimental data indicated as confidence intervals in the plot), which indicates that a uniform coating was obtained with the absence of plugs or necks, where the pressure drop was expected to be the highest.

Fig. 6. (a) Distribution of the TiO_2 coating thickness obtained in the 250 μm fused silica capillaries using different precursor sol concentrations. Displacement speed: 0.2 mm/s. Oven temperature: 450 K. (b) The comparison of the average coating thickness determined by (●) SEM and (♦) hydrodynamic study.

For capillaries with smaller internal diameters, solid plugs are likely to be formed due to capillary forces[28], but the coating method reported can be applied to coat capillaries with larger diameters. For a given TiO_2 precursor concentration, the coating thickness is proportional to the internal diameter of the capillary (Fig. 7) allowing one to obtain coating thickness above 10 μm in the tubes about 1 mm in diameter in a single deposition step.

Fig. 7. Effect of the capillary inner diameter on the coating thickness (SEM data) using a 80 g/L TiO_2 sol.

Semihydrogenation in the capillary reactor

In order to test the coating method for catalytic applications, MBY semihydrogenation on the Bi-poisoned Pd catalyst was performed. To prepare the catalyst, a dispersion of unsupported Pd-Bi nanoparticles was mixed with a 80 g/L TiO_2 sol in a 1:1 volume ratio and the mixture was deposited onto the inner walls of a 2.5-m silica capillary with an internal diameter of 530 μm. After thorough surfactant extraction with ethanol followed by drying, a coating thickness of 3.6±1.1 μm was obtained with a nominal Pd loading of 3.3 wt%, and a total catalyst loading of 5 mg/m. During the parameter optimisation, the solution flow rate was varied in the interval of 30-50 μL/min at a constant hydrogen gas flow rate of 10 mL/min (STP), which corresponded to superficial flow velocities of 2-4 mm/s for liquid and 0.75 m/s for hydrogen. Reynolds numbers were below 5 showing laminar liquid and gas flows. Image analysis showed that a slug-annular flow regime was realised.[46,47]

Fig. 8 shows the performance of the capillary microreactor in the hydrogenation of a 1200 mol/m^3 MBY solution in hexane at reaction temperatures of 310 and 335 K. As the flow rate increased, the MBY conversion decreased due to shorter residence time, while the selectivity towards MBE increased reaching 98 % at MBY conversion up to 80 %. Importantly, even at high MBY conversions, the MBE selectivity was high, allowing for a maximum MBE yield of 95.0 and 94.3 % at 335 and 310 K, respectively.

The very high selectivity observed on the Pd-Bi catalyst can be explained by a combination of thermodynamic effects and active site poisoning. The former means the displacement of alkene species from the catalyst surface due to much higher heat of adsorption of alkynes which results in about 90-95 % alkene selectivity over monometallic Pd catalysts.[48–51] The latter, poisoning of Pd catalysts with Bi, further increased selectivity by blocking the step and edge sites of the Pd nanoparticles, as those sites are responsible for over hydrogenation of MBY molecules.[40,48,52]

Fig. 8. Summary of the performance of the capillary microreactor with Pd-Bi/TiO_2 in MBY semihydrogenation (1200 mol/m^3 MBY in hexane, 10 mL/min (STP) H_2 flow, (a) 310 K and (b) 335 K). Selectivity is calculated towards MBE.

A high long term stability is required for industrial applications of the microreactor. The catalyst stability was studied at 335 K using an MBY solution flow rate of 42.5 μL/min and a hydrogen flow of 10 mL/min for 100 hours. Fig. 9 shows that the MBE yield was 93±1.5 % with neither deactivation nor decrease in selectivity observed. However, there were some fluctuations in the product yield, also observed during the parametric study (Fig. 8). These are likely related to minor fluctuations in the flow rates, the thermostat temperature (about ±0.5 K), and the pressure drop in the reactor due to hydrodynamic reasons.[53]

Fig. 9. Long-term stability of the capillary microreactor with Pd-Bi/TiO_2 in MBY semihydrogenation (1200 mol/m^3 MBY in hexane flow 42.5 μL/min, 10 mL/min (STP) H_2 flow, 335K).

Interestingly, it can be seen from Fig 8 that the reaction temperature had a marginal effect on MBY conversion. In particular, the maximum MBE yield was observed at almost the same liquid flow rates of 40.0 and 42.5 μL/min at 310 and 335 K, respectively, showing very close apparent reaction rates (Fig. 8). However, an increase in the hydrogenation reaction rate by a factor of 2.5 would be expected

at 335 K as compared with 310 K,[54,55] which should lead to much higher conversion at a given liquid flow rate. This observation can be explained by either (i) a substantial decrease in the hydrogen partial pressure due to solvent evaporation and diffusion to the gas phase, (ii) mass-transfer limitations, or (iii) a combination of these factors.

The observed small change in the hydrogenation reaction rates with the temperature increase (Fig. 9) can be explained by the effect of hexane evaporation. The partial pressures of hexane at 310 and 335 K was estimated by the Antonie equation to be 0.33 and 0.81 bar,[56] which correspond to the hydrogen partial pressures of 0.97 and 0.49 bar, respectively. Because the hydrogenation is a first order reaction in hydrogen,[55] the reaction rate was expected to decrease by a factor of 2.3 with a temperature increase from 310 to 335 K due to hydrogen dilution (Electronic Supplementary Information). As a result, the increase in intrinsic reaction rate due to higher temperature was expected to be balanced by its decrease due to lower hydrogen pressure.

In order to study the effects of mass transfer and solvent evaporation experimentally, the hydrogenation was performed in a toluene solution. Toluene is a less volatile solvent, resulting in similar hydrogen pressures of 1.23 and 1.10 bar at 310 and 335 K, respectively. For the MBY solution in toluene, the effect of solvent evaporation was expected to be less pronounced, while its viscosity similar to that of hexane provided similar hydrodynamic behaviour. Hence, a significant increase of the hydrogenation rate at higher temperatures is expected in toluene.

Fig. 10. (a) MBE maximum yield as a function of the reaction temperature and the MBY solution flow rate. (b) Corresponding hydrogen consumption by MBY (1200 mol/m^3 MBY in toluene, 10 mL/min (STP) H_2 flow).

Fig. 10a shows the MBE yield as a function of liquid flow rate at three reaction temperatures obtained for the MBY hydrogenation in toluene. Similar to the hexane solution (Fig. 8), the MBE yield at the reaction temperature of 310 K achieved a maximum at a liquid flow rate of about 40 μL/min, where the product of MBY conversion and the MBE selectivity was the highest. At higher reaction temperatures, however, a significant increase in the reaction rate was observed. At 335 K, MBE was further hydrogenated consuming more than 1 mol of hydrogen per mol of MBY in the entire flow rate range studied, while at 350 K, the fully hydrogenated product was obtained leading to zero MBE yield at a flow rate up to 45 μL/min (Fig. 10b). Importantly, the apparent hydrogenation reaction rates increased by 130 % with the temperature increase from 310 to 335 K, which is in good agreement with the reported kinetic studies of hydrogenation.[54,55] Considering external mass transfer limitations, the

reaction rate was expected to be proportional to temperature in the power of 0.75,[57] leading to apparent reaction rate increase of less than 10 % in the studied temperature range, showing that mass transfer limitations did not apply for the studied capillary reactor. Furthermore, Warnier shown that external mass transfer limitations cannot be reached prior to reaching internal (pore) limitations in the semi-hydrogenation in capillary microreactors.[58]

In order to estimate pore diffusion, the Thiele modulus (ϕ) was calculated according to equation (1), where *d* is the average coating thickness, D_{eff} - efficient diffusion coefficient of hydrogen though the catalyst pores and k_v - overall volumetric rate constant.[59]

$$\phi = d\sqrt{k_v / D_{eff}} \qquad (1)$$

The efficient diffusion coefficient of hydrogen in the catalyst pores was estimated to be 10^{-9} m^2 s^{-1} as described by Vannice.[60,61] The overall volumetric rate constant was calculated using equation (2),

$$k_v = \frac{-\Delta F_{MBY}}{A\,L}\frac{H}{p_{H2}} \qquad (2)$$

where ΔF_{MBY} is the change in the MBY molar concentration in the reactor of the length *L* and cross-section *A*; H is Henry constant (in Pa m^3 mol^{-1}) of hydrogen solubility in hexane[62,63] and p_{H2} hydrogen partial pressure estimated earlier for hexane solution.

A high-boundary estimation of the overall volumetric rate constant in the hexane solution at 335 K provided a value of 0.6 s^{-1}, resulting in the value of Thiele modulus of 0.089 and the effectiveness factor ($\eta = \tanh(\phi)/\phi$) of 0.997. The value of the effectiveness factor very close to 1 shows that there is no internal mass transfer limitations.[59] Because the concentration of the reactant in liquid phase is 2 orders of magnitude higher than that of hydrogen, internal diffusion of organic species is not a limiting step either. Furthermore, very high alkene selectivity observed in the work could not be reached in case of pore diffusion limitations of the liquid reactant.[64] It confirms the conclusion that mass transfer limitations did not apply, and the reactions were controlled by intrinsic kinetics of the hydrogenation reaction.

Table 1. Comparison of the microreactor performance in semihydrogenation

Reference	Reactor	Catalyst	Alkyne	Max. alkene yield, %	R_{app}[a], µmol s^{-1}	R_{vol}[b], µmol	R_{cat}[c], µmol

						m_{react}^{-3} s^{-1}	s^{-1} kg_{cat}^{-1}
Rebrov et al.[23]	Capillary	Pd/TiO_2	PA[d]	80.3	65	148	53
Rebrov et al.[29]	Capillary	$PdZn/TiO_2$	MBY	89.5	23	46	38
		$PdZn/TiO_2$ + pyridine	MBY	97.0	19	38	32
Liguori and Barbaro[65]	Monolith	Pd@MonoBor	MBY	86.4	1000	5680	34
		Pd@MonoBor	PA[d]	93.7	166	950	6
Current work	Capillary	$PdBi/TiO_2$	MBY	93.0±1.5	850	1540	64

[a] Reactor alkyne hydrogenation performance; [b] Performance normalized for the reaction volume; [c] Performance normalized per kg of the catalyst; [d] Phenylacetylene

Conclusions

A novel method for the controlled deposition of micrometre-thick mesoporous titania coatings inside long capillary microreactors is proposed. The two main advantages of the method over the conventional static coating procedure are associated with the use of elevated temperature and introduction of the capillary at a constant displacement speed into the oven. Elevated deposition temperature prevents capillary clogging even with concentrated solutions, while the displacement speed controls the evaporation rate. This allows very slow solvent removal leading to the formation of uniform coatings. The coating thickness can be precisely controlled and it is proportional to the sol concentration and the internal diameter of the capillary, while textural properties can be adjusted with a surfactant.[43] Although only titania coatings were investigated in this work, the method can be extended to the deposition of any thermostable materials, particularly metal oxide sols.

The method was applied to coat the inner walls of a capillary microreactor (i.d. 0.53 mm, 2.5 m long) with a titania supported Bi-poisoned Pd catalyst. The microreactor demonstrated exceptionally high selectivity in semihydrogenation of MBY with the alkene yield up to 95 % and with no observed catalyst deactivation for a time on stream of 100h. The alkyne hydrogenation performance was significantly higher than for the previously reported capillary microreactors (Table 1).

The capillary microreactor produced in this work offers opportunities for further intensive and extensive performance improvement using high hydrogen pressure, selective microwave catalyst heating, increasing the reactor length and the coating thickness or by numbering-up. Capillary microreactors open a promising and cost-efficient way for the replacement of traditional, energy- and

labour-inefficient batch reactor systems in the synthesis of high-value pharmaceutical and fine chemistry products.

Acknowledgements

Authors are grateful to Dr. C. Willies, Dr. R. Lewis, Dr. M. Hird, Professor P. Fletcher and Professor B. Binks for the access to their equipment, to the EU for an FP7 Grant for the MAPSYN Project (MAPSYN.eu No. CP-IP 309376) and Royal Society for an International Joint Project Grant 2010/R.

References

1. L. Liu and X. Chen, *Chem. Rev.*, 2014, **114**, 9890–9918.
2. Y. Shiraishi, D. Tsukamoto, Y. Sugano, A. Shiro, S. Ichikawa, S. Tanaka, and T. Hirai, *ACS Catal.*, 2012, **2**, 1984–1992.
3. H. Chen, C. E. Nanayakkara, and V. H. Grassian, *Chem. Rev.*, 2012, **112**, 5919–48.
4. P. Pfeifer, T. Zscherpe, K. Haas-Santo, and R. Dittmeyer, *Appl. Catal. A Gen.*, 2011, **391**, 289–296.
5. T. Fröschl, U. Hörmann, P. Kubiak, G. Kučerová, M. Pfanzelt, C. K. Weiss, R. J. Behm, N. Hüsing, U. Kaiser, K. Landfester, and M. Wohlfahrt-Mehrens, *Chem. Soc. Rev.*, 2012, **41**, 5313–60.
6. Z. Li, B. Gao, G. Z. Chen, R. Mokaya, S. Sotiropoulos, and G. Li Puma, *Appl. Catal. B Environ.*, 2011, **110**, 50–57.
7. A. M. Ramirez, K. Demeestere, N. De Belie, T. Mäntylä, and E. Levänen, *Build. Environ.*, 2010, **45**, 832–838.
8. K. Jähnisch, V. Hessel, H. Löwe, and M. Baerns, *Angew. Chemie*, 2004, **43**, 406–46.
9. M. Irfan, T. N. Glasnov, and C. O. Kappe, *ChemSusChem*, 2011, **4**, 300–16.
10. V. Hessel, G. Cravotto, P. Fitzpatrick, B. S. Patil, J. Lang, and W. Bonrath, *Chem. Eng. Process. Process Intensif.*, 2013, **71**, 19–30.
11. D. Reay, C. Ramshaw, and A. Harvey, *Process intensification: Engineering for efficiency, sustainability and flexibility*, Butterworth-Heinemann, 2011.
12. G. Chen, J. Yue, and Q. Yuan, *Chinese J. Chem. Eng.*, 2008, **16**, 663–669.
13. V. Hessel, D. Kralisch, N. Kockmann, T. Noël, and Q. Wang, *ChemSusChem*, 2013, 6, 746–789.
14. J. R. Burns and C. Ramshaw, *Lab Chip*, 2001, **1**, 10–5.
15. K. F. Jensen, *Chem. Eng. Sci.*, 2001, **56**, 293–303.
16. D. van Herk, P. Castaño, M. Makkee, J. A. Moulijn, and M. T. Kreutzer, *Appl. Catal. A Gen.*, 2009, **365**, 199–206.
17. M. W. Losey, M. A. Schmidt, and K. F. Jensen, *Ind. Eng. Chem.*, 2001, **40**, 2555–2562.
18. B. P. Mason, K. E. Price, J. L. Steinbacher, A. R. Bogdan, and D. T. McQuade, *Chem. Rev.*, 2007, **107**, 2300–18.
19. A.-K. Liedtke, F. Bornette, R. Philippe, and C. de Bellefon, *Chem. Eng. J.*, 2013, **227**, 174–181.
20. J. Kobayashi, Y. Mori, K. Okamoto, R. Akiyama, M. Ueno, T. Kitamori, and S. Kobayashi, *Science*, 2004, **304**, 1305–8.
21. R. J. White, R. Luque, V. L. Budarin, J. H. Clark, and D. J. Macquarrie, *Chem. Soc. Rev.*, 2009, **38**, 481–94.

22. J. A. Schwarz, C. Contescu, and A. Contescu, *Chem. Rev.*, 1995, **95**, 477–510.
23. E. V Rebrov, A. Berenguer-Murcia, H. E. Skelton, B. F. G. Johnson, A. E. H. Wheatley, and J. C. Schouten, *Lab Chip*, 2009, **9**, 503–6.
24. L. E. Scriven, *MRS Proc.*, 1988, **121**, 717–729.
25. M. Faustini, B. Louis, P. A. Albouy, M. Kuemmel, and D. Grosso, *J. Phys. Chem. C*, 2010, **114**, 7637–7645.
26. N. Krins, M. Faustini, B. Louis, and D. Grosso, *Chem. Mater.*, 2010, **22**, 6218–6220.
27. G. I. Taylor, *J. Fluid Mech.*, 1961, **10**, 161–165.
28. J. Bravo, A. Karim, T. Conant, G. P. Lopez, and A. Datye, *Chem. Eng. J.*, 2004, **101**, 113–121.
29. E. V Rebrov, E. A. Klinger, A. Berenguer-Murcia, E. M. Sulman, and J. C. Schouten, *Org. Process Res. Dev.*, 2009, **13**, 991–998.
30. S.-M. Hwang, O. J. Kwon, and J. J. Kim, *Appl. Catal. A Gen.*, 2007, **316**, 83–89.
31. J. F. Ng, Y. Nie, G. K. Chuah, and S. Jaenicke, *J. Catal.*, 2010, **269**, 302–308.
32. M. Ueno, T. Suzuki, T. Naito, H. Oyamada, and S. Kobayashi, *Chem. Commun.*, 2008, 1647–9.
33. J. Mitrovic, *Chem. Eng. Sci.*, 2012, **75**, 279–281.
34. G. Lambertus, A. Elstro, K. Sensenig, J. Potkay, M. Agah, S. Scheuering, K. Wise, F. Dorman, and R. Sacks, *Anal. Chem.*, 2004, **76**, 2629–37.
35. S. Reidy, G. Lambertus, J. Reece, and R. Sacks, *Anal. Chem.*, 2006, **78**, 2623–2630.
36. K. J. Grob and K. Grob, *Chromatographia*, 1977, **10**, 250–255.
37. K. Grob and G. Grob, *J. High Resolut. Chromatogr.*, 1983, **6**, 133–139.
38. W. Bonrath, J. Medlock, J. Schutz, B. Wüstenberg, and T. Netscher, *Hydrogenation in the vitamins and fine chemicals industry – an overview, In: I. Karame (Ed.) Hydrogenation, InTech, Rijeka, 2012, pp. 69-90.*, InTech, 2012.
39. B. Bridier, N. López, and J. Pérez-Ramírez, *Dalt. Trans.*, 2010, **39**, 8412–9.
40. J. A. Anderson, J. Mellor, and R. K. P. K. Wells, *J. Catal.*, 2009, **261**, 208–216.
41. B. Bradley, M. Singleton, and A. L. Wan Po, *J. Clin. Pharm. Ther.*, 1989, **14**, 423–441.
42. J. Sá, J. Montero, E. Duncan, and J. A. Anderson, *Appl. Catal. B Environ.*, 2007, **73**, 98–105.
43. R. Bleta, P. Alphonse, and L. Lorenzato, *J. Phys. Chem. C*, 2010, **114**, 2039–2048.
44. R. W. Lockhart and R. C. Martinelli, *Chem. Eng. Prog.*, 1949, **45**, 39–48.
45. D. Chisholm, *Int. J. Heat Mass Transf.*, 1967, 10, 1767–1778.
46. N. Shao, A. Gavriilidis, and P. Angeli, *Chem. Eng. Sci.*, 2009, **64**, 2749–2761.
47. J. Yue, G. Chen, Q. Yuan, L. Luo, and Y. Gonthier, *Chem. Eng. Sci.*, 2007, **62**, 2096–2108.
48. M. Crespo-Quesada, A. Yarulin, M. Jin, Y. Xia, and L. Kiwi-Minsker, *J. Am. Chem. Soc.*, 2011, **133**, 12787–94.
49. A. N. R. Bos and K. R. Westerterp, *Chem. Eng. Process. Process Intensif.*, 1993, **32**, 1–7.
50. K. Reuter and M. Scheffler, *Phys. Rev. B*, 2006, **73**, 1–17.
51. A. Borodziński and G. C. Bond, *Catal. Rev.*, 2006, **48**, 91–144.
52. J. A. Bennett, G. A. Attard, K. Deplanche, M. Casadesus, S. E. Huxter, L. E. Macaskie, and J. Wood, *ACS Catal.*, 2012, **2**, 504–511.
53. V. van Steijn, M. T. Kreutzer, and C. R. Kleijn, *Chem. Eng. J.*, 2008, **135**, S159–S165.
54. M. Crespo-Quesada, M. Grasemann, N. Semagina, A. Renken, and L. Kiwi-Minsker, *Catal. Today*, 2009, **147**, 247–254.
55. N. Semagina, E. Joannet, S. Parra, E. Sulman, A. Renken, and L. Kiwi-Minsker, *Appl. Catal. A Gen.*, 2005, **280**, 141–147.
56. G. F. Carruth and R. Kobayashi, *J. Chem. Eng. Data*, 1973, **18**, 115–126.
57. S. Walter, S. Malmberg, B. Schmidt, and M. A. Liauw, *Catal. Today*, 2005, **110**, 15–25.
58. M. J. F. Warnier, Ph.D. thesis, University of Eidhoven, 2009.
59. G. F. Froment, K. B. Bischoff, and J. De Wilde, *Chemical reactor analysis and design, 3rd Edition*, John Wiley & Sons, Inc., 2011.

60. M. A. Vannice, *Kinetics of catalytic reactions*, Springer Science+Business Media, New York, 2005.
61. C. R. Wilke and P. Chang, *AIChE J.*, 1955, **1**, 264–270.
62. M.-S. Fu and C.-S. Tan, *Fluid Phase Equilib.*, 1994, **93**, 233–247.
63. T. Katayama and T. Nitta, *J. Chem. Eng. Data*, 1976, **21**, 194–196.
64. T. A. Nijhuis, G. van Koten, and J. A. Moulijn, *Appl. Catal. A Gen.*, 2003, **238**, 259–271.
65. F. Liguori and P. Barbaro, *J. Catal.*, 2014, **311**, 212–220.